

RXTE Observation of Cygnus X-1: I. Spectral Analysis

James B. Dove^{1,2*}, Jörn Wilms^{3,1}, Michael A. Nowak¹,
Brian A. Vaughan⁴, and Mitchell C. Begelman^{1,2}

¹ *JILA, University of Colorado and National Institute of Standards and Technology, Campus Box 440, Boulder, CO 80309-0440, USA*

² *Department of Astrophysical and Planetary Sciences, University of Colorado, Boulder, CO 80309-0391, USA*

³ *Institut für Astronomie und Astrophysik, Abt. Astronomie, Waldhäuser Str. 64, D-72076 Tübingen, Germany*

⁴ *Space Radiation Laboratory, California Institute of Technology, 220-47 Downs, Pasadena, CA 91125, USA*

1 February 2008

ABSTRACT

We present the results of the analysis of the broad-band spectrum of Cygnus X-1 from 3.0 to 200 keV, using data from a 10 ksec observation by the *Rossi X-ray Timing Explorer*. The spectrum can be well described phenomenologically by an exponentially cut-off power law with a photon index $\Gamma = 1.45^{+0.01}_{-0.02}$ (a value considerably harder than typically found), e-folding energy $E_f = 162^{+9}_{-8}$ keV, plus a deviation from a power law that formally can be modeled as a thermal blackbody with temperature $kT_{\text{BB}} = 1.2^{+0.0}_{-0.1}$ keV. Although the 3–30 keV portion of the spectrum can be fit with a reflected power law with $\Gamma = 1.81 \pm 0.01$ and covering fraction $f = 0.35 \pm 0.02$, the quality of the fit is significantly reduced when the HEXTE data in the 30–100 keV range is included, as there is no observed hardening in the power law within this energy range. As a physical description of this system, we apply the accretion disc corona models of Dove, Wilms & Begelman (1997a) — where the temperature of the corona is determined self-consistently. A spherical corona with a total optical depth $\tau = 1.6 \pm 0.1$ and an average temperature $kT_c = 87 \pm 5$ keV, surrounded by an exterior cold disc, does provide a good description of the data ($\chi^2_{\text{red}} = 1.55$). These models deviate from the data by up to 7% in the 5–10 keV range, and we discuss possible reasons for these discrepancies. However, considering how successfully the spherical corona reproduces the 10–200 keV data, such “photon-starved” coronal geometries seem very promising for explaining the accretion processes of Cygnus X-1.

Key words: radiation mechanisms: non-thermal – radiative transfer – X-rays: binaries – accretion, accretion discs

1 INTRODUCTION

Cygnus X-1 is one of the most firmly established persistent galactic black hole candidates (BHCs). Since it is also one of the brightest BHCs, the study of its X-ray spectrum can help reveal the physical conditions of the inner region around accreting compact objects. The X-ray spectrum of Cyg X-1 while in the hard (i.e., low) state can be roughly described by a power-law with a photon-index $\Gamma \sim 1.65$, modified by an exponential cutoff with an e-folding energy $E_f \sim 150$ keV (Ebisawa et al. 1996; Gierliński et al. 1997, and references therein). A spectral shape of this form is naturally explained by Comptonization of low-energy seed photons by a semi-relativistic corona (Sunyaev & Trümper 1979; Titarchuk 1994). Below about 1 keV, there is evidence for a soft-excess,

usually interpreted as thermal radiation from a cold accretion disc having a temperature $kT_{\text{BB}} \sim 0.1 - 0.3$ keV (Bahucińska-Church et al. 1995; Ebisawa et al. 1996). In addition, the spectrum is usually found to contain a weak iron line feature at ≈ 6.4 keV and a slight hardening above 10 keV, often interpreted as being due to Compton reflection (Barr, White & Page 1985; Ebisawa et al. 1996, and references therein).

The combination of a Comptonization continuum and reprocessing features has been interpreted as being due to an accretion disc corona (ADC). The geometric configuration of the corona and the cold disc, however, is still unclear. In most prior work, the geometry has been assumed to be a cold accretion disc embedded between two hot coronae, with a slab geometry (Haardt, Maraschi & Ghisellini 1996; Haardt et al. 1993, and references therein). Recently, however, evidence has been presented showing that ADC models with a slab geometry suffer from several problems, making them less likely to be the appropriate models for ex-

* Present address: Department of Physics and Astronomy, University of Wyoming, Laramie, WY 82071, USA

plaining the high-energy radiation of BHCs. Gierliński et al. (1997) analyzed simultaneous *Ginga*-OSSE data of Cyg X-1 and found that the strength of the reflection component is too small to be consistent with a slab geometry. Using a non-simultaneous broad-band spectrum of Cyg X-1, we previously argued that our self-consistent ADC models with a slab geometry (in which the coronal temperature is not a free parameter but is determined by balancing Compton cooling with viscous dissipation) could not have a high enough temperature* to explain both the observed power-law and exponential cutoff (Dove, Wilms & Begelman 1997a; Dove et al. 1997b; Wilms et al. 1997). Moreover, the luminosity of the disc expected due to reprocessing is comparable to the coronal luminosity, and therefore the predicted soft-excess component is much stronger than that observed (Dove et al. 1997b; Gierliński et al. 1997).

Most of the problems cited above are due to the cold disc of the slab ADC model having a covering fraction of unity (i.e., all downward directed coronal radiation is reprocessed in the cold disc). ADCs having a geometry with a smaller covering fraction have weaker reprocessing features, are less efficiently Compton cooled, and thereby allow higher coronal temperatures for a given τ . An example is a hot coronal sphere that is surrounded by an exterior cold, optically thick, geometrically thin, accretion disc (called the “sphere+disc geometry” henceforth), similar to the two-temperature disc model of Shapiro, Lightman & Eardley (1976) and to advection dominated models (Abramowicz et al. 1995; Chen 1995; Narayan & Yi 1994). Based on non-simultaneous BBXRT, Mir-TTM, Mir-HEXE, and OSSE data, we have shown that the sphere+disc ADC model can explain the observed spectrum of Cyg X-1 for energies in the ~ 1 keV–1 MeV range (Dove et al. 1997b).

In this paper, we analyze the broad-band spectrum of Cyg X-1 from 3.0 to 200 keV, using data from the *Ross X-ray Timing Explorer* (RXTE). The simultaneity of this broad-band observation allows us to place stronger constraints on the coronal parameters than was previously possible. In §2, we describe the observations performed and the procedures used in the data analysis. In §3, we give the results from spectral modeling of the Cyg X-1 spectrum using both “standard” simplified models as well as our self-consistent ADC models. In §4 the results of these fits are discussed.

2 OBSERVATIONS AND DATA ANALYSIS

RXTE observed Cyg X-1 for a total of 22.5 ksec on 1996 October 23 and 24. For the analysis presented here, we use data from the proportional counter array (PCA) and the high energy X-ray timing experiment (HEXTE). The PCA consists of five Xe proportional counters with a total effective area of about 6500 cm² (Zhang et al. 1993), while HEXTE consists of two clusters of NaI(Tl)/CsI scintillation counters with a total effective area of about 1400 cm² (Rothschild et al. 1997). For both instruments, only data where the source

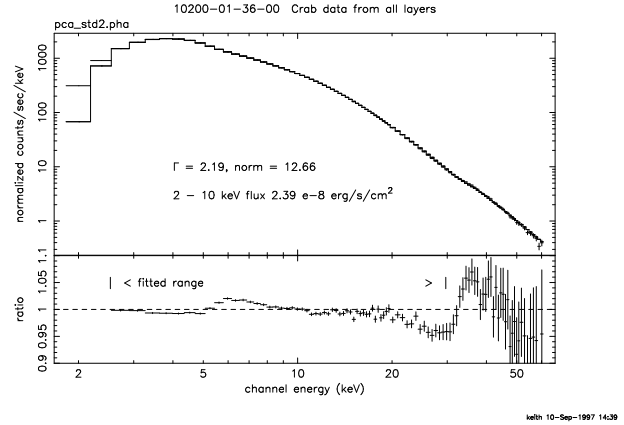


Figure 1. Top: Comparison of the Crab Pulsar spectrum, taken by PCA, to the best fit power law model. Bottom: Ratio of the residuals of the model to the data (data/model). Figure by K. Jahoda, private communication.

was observed at elevations higher than 10° above the spacecraft horizon were used. Due to missing standard-mode PCA data, we have used only the first 10 ksec of the observation. This duration is sufficient for the spectral analysis, as the PCA count-rate is high (≈ 4300 cps, with a background of ≈ 150 cps).

For the extraction of the PCA data, we used the standard RXTE ftools, version 4.0. We used version 1.5 of the background estimator program, in which activation due to the South Atlantic Anomaly and an estimate for the internal background based on the measurement of the rate of Very Large Events within the PCA are taken into account. To this estimation, the measured diffuse X-ray background is added by the program. The comparison of the modeled background spectrum to the background measured by the PCA during the Earth occultation phases of the observation (defined by an elevation $< -5^\circ$) indicates that the background model count-rate has an uncertainty of 5 to 10% (i.e., $\lesssim 0.3\%$ of the total count rate). The use of the background model is still preferable to using the Earth occultation data because the latter method cannot estimate the variation of the background due to the variation of the rigidity of the Earth’s magnetic field during on-source time intervals.

For the spectral analysis of the PCA we used version 2.2.1 of the PCA response matrix (Jahoda, priv. comm.; for an overview of the PCA calibration issues see Jahoda et al., 1996). The PCA response matrix is now fairly well understood. An analysis of the residuals of a standard power-law fit to the spectrum of the Crab pulsar indicates that the uncertainty of the calibration in the vicinity of the Xenon L edge (around 5.5 keV) is about 2%. This makes a precise determination of the parameters of the Fe K α line difficult. In addition, the Crab fit indicates a calibration uncertainty of about 5% above ≈ 30 keV, as shown in Figure 1. Since HEXTE provides reliable data for energies $\gtrsim 20$ keV we ignored the PCA data above 30 keV. To be conservative, we ignored the first four PCA channels (i.e., we only included PCA data above 3 keV). To account for the additional uncertainties in the PCA response matrix, a 2% systematic error was added to all PCA data.

Software provided by the HEXTE instrument group was

* Formally, a high temperature is possible for a slab corona if the coronal optical depth is very low. However, such low optical depth coronae also produce spectra that are too soft to explain the observations of Cyg X-1.

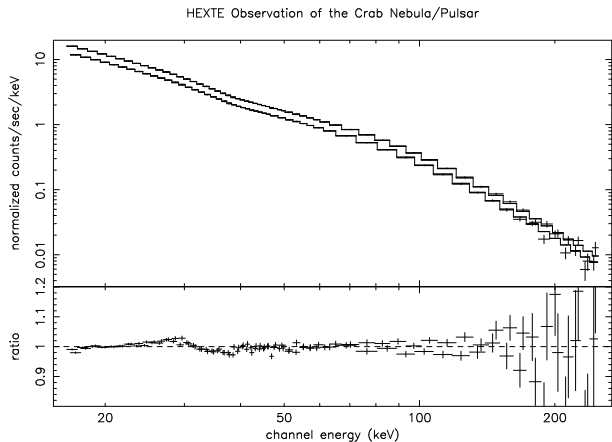


Figure 2. Top: Comparison of the Crab Pulsar spectrum, taken simultaneously by HEXTE Clusters A and B, to the best fit broken power law model ($\Gamma_1 = 2.045 \pm 0.002$, $\Gamma_2 = 2.140 \pm 0.009$, and the break energy $E_B = 57.2 \pm 3.0$ keV). Bottom: Ratio of the residuals of the model to the data (data/model) (Rothschild et al. 1997, Fig. 11).

used for the extraction of the HEXTE data and subsequent dead-time corrections. Since HEXTE is source-background swapping, the background is not a problem in the data analysis. We used the HEXTE response matrices released 1997 March 20. Only data above 20 keV were used due to the uncertainty of the response matrix below these energies. At high energies, the spectrum was cut at 200 keV. To ensure good statistical accuracy above 50 keV, the spectrum was rebinned by a factor of 3 for channels between 50 and 100 keV, and by a factor of 10 for higher channels. The spectrum of the Crab Pulsar, taken by HEXTE, is shown in Figure 2.

3 SPECTRAL ANALYSIS

3.1 Standard Models

Spectral fitting was first performed using the following standard models: a power-law, a power-law with an exponential cutoff, a power-law with an exponential cutoff plus a cold reflection component, and thermal Comptonization models. In addition, we added a Gaussian line (with energy and width fixed to 6.4 keV and 0.1 keV, respectively) to several of these models. We fixed the low-energy absorption to an equivalent cold Hydrogen column of $N_H = 6 \times 10^{21} \text{ cm}^{-2}$, the value suggested by the soft X-ray spectrum and interstellar reddening measurements of HDE 226868 (Bahucińska & Hasinger 1991; Wu et al. 1982). The results of the spectral fits are given in Table 1[†].

For energies $E \gtrsim 10$ keV, a power-law with an exponential cutoff provides a good description of the data, as also shown in Figure 3. The value for the e-folding energy, E_f ,

[†] To account for the known discrepancies in the relative normalization of PCA and HEXTE, we introduced a multiplicative constant in the spectral models that represents the relative normalization between the data-sets. The relative normalization between HEXTE and PCA was always found to be 0.74 ± 0.01 and is therefore not listed in Table 1.

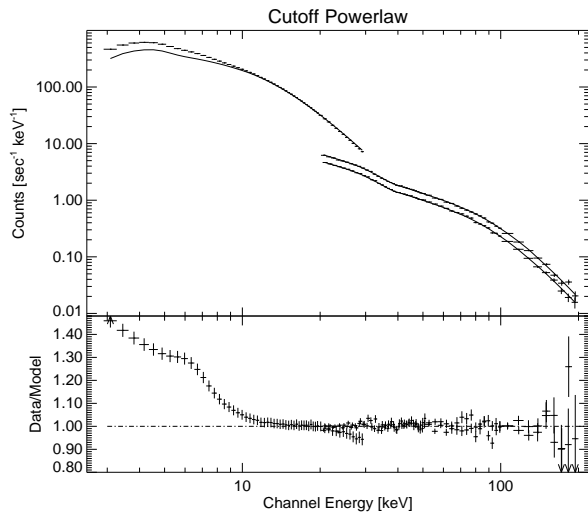


Figure 3. Comparison of the RXTE spectrum of Cyg X-1 to the best-fit power-law with an exponential cutoff model. This model was fit to only the 10 - 200 keV data, yielding $\chi^2_{\text{red}} = 171/149$. The photon power-law index $\Gamma = 1.46$ and the e-folding energy $E_f = 168$ keV. A soft-excess below 10 keV is clearly evident.

is well constrained due to the quality of the HEXTE data. The analysis of the residuals of this fit indicates the presence of a soft excess at energies $\lesssim 8$ keV, as shown in Figure 3. Adding a black-body component with a temperature $kT_{\text{BB}} \approx 1$ keV and a Gaussian component, with an equivalent width $\text{EW} = 46.4$ eV, to the model improves the quality of the fit, resulting in a good description of the data over the whole energy range ($\chi^2_{\text{red}} = 170/166$), as shown in Figure 4. We note that this black-body component should not be interpreted literally as being due to disc emission; it is simply added phenomenologically to measure the magnitude of the data's deviation from a power law. We could have instead used a disc blackbody, Gaussian, or bremsstrahlung model with roughly equal success.

The addition of a reflection component to this model *does not* improve the quality of the fit, as the best-fit value for the fraction of incident radiation that is Compton reflected by cold matter is $f \lesssim 0.02$. Even though we only considered PCA data in the 3.0 keV – 30 keV range, the power-law index of the continuum is well constrained by the HEXTE data, and there is no evidence that the spectral slope of the data for the two instruments disagree within the energy range of the overlap. The PCA residuals between 20 and 30 keV seen in Figures 3-6 are consistent with those seen for power-law fits to the Crab, as shown in Figure 1.

We believe that the measured spectrum parameters, which represent a harder power law and a weaker reflection component than previously found by others, is mostly due to our fitting the entire 3 – 200 keV spectral band. Previous observations using different instruments have had relatively poor spectral coverage in the energy range $\sim 30 - 100$ keV. We do not believe that our results are heavily influenced by any remaining uncertainties in the PCA response matrix. To support this claim, if we restrict the data to 3 – 30 keV and 100 – 200 keV (roughly covering the energy range of the *Ginga* + OSSE observations) we *do* find best-fit param-

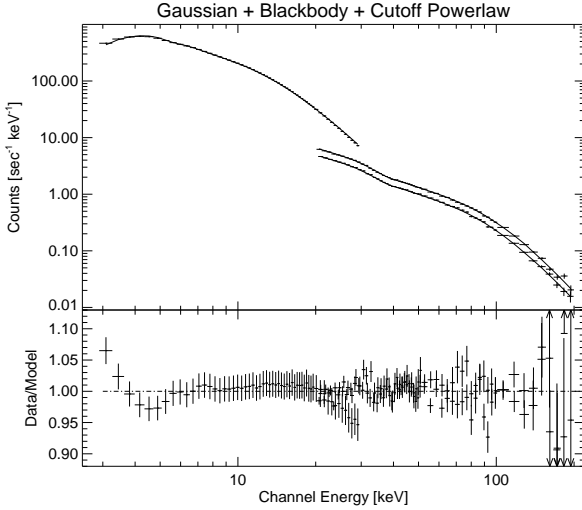


Figure 4. Comparison of the RXTE spectrum of Cyg X-1 to the best-fit power-law with an exponential cutoff model. The photon power-law index $\Gamma = 1.45$ and the e -folding energy is $E_f = 164$ keV. A blackbody component, with a temperature $kT_{\text{BB}} = 1.1$ keV and a relative flux of $\lesssim 5\%$, and a Gaussian component, with an energy fixed at 6.4 keV and an equivalent width $EW = 46.4$ eV, were added to fit the soft-excess. For this fit, $\chi^2_{\text{red}} = 170/166$.

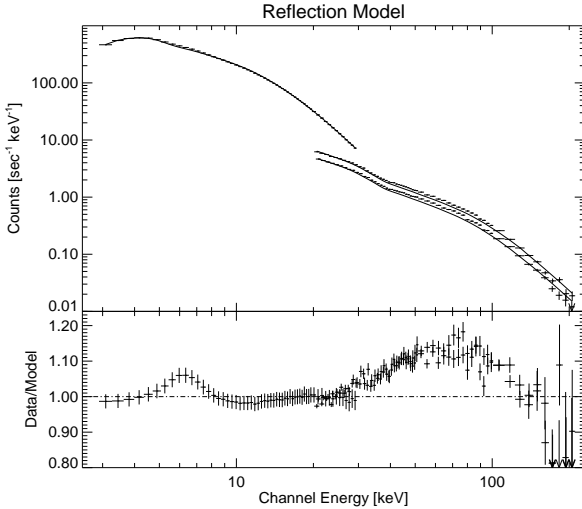


Figure 5. Top: Comparison of the reflection model (Magdziarz & Zdziarski 1995) to the PCA data alone. Here, $\chi^2_{\text{red}} = 143/73$. Adding a Gaussian component, with a line energy $E_l = 6.4$ keV, a line width $\Delta E = 64$ eV, and an equivalent width $EW = 110$ eV, results in a slightly better fit ($\chi^2_{\text{red}} = 107/72$), and the other best-fit parameters do not change appreciably. Bottom: Ratio between data and model.

eter values similar to those previously found for Cyg X-1. Specifically, for this restricted data range, we find that a reflected power law with $\Gamma = 1.81 \pm 0.01$ and covering fraction $f = 0.35 \pm 0.02$ yields $\chi^2_{\text{red}} = 157/90 = 1.75$. Adding back the HEXTE data in the 30–100 keV range, significantly reduces the quality of the fit ($\chi^2_{\text{red}} = 8.7, 77$ dof), as shown in Figure 5. Being able to fit a reflected power-law with a large

disc covering fraction is thus seen to be partly a consequence of ignoring the data in the $\sim 30 - 100$ keV range.

It is this 30–100 keV energy range that is crucial for constraining a power-law index since these energies are uncontaminated by reprocessing or reflection features, i.e., the final power law in this energy range is identical to the intrinsic power law prior to reflection. We therefore postulate that the observed 10–30 keV “hardening” feature typically found by others appears to be the beginning of a hard power-law that continues to ~ 100 keV, and that the $\sim 1 - 10$ keV portion of the spectrum is softer due to contamination from the thermal excess. This contamination could be due to Comptonization of the thermal radiation emitted by the cold disc with an effective blackbody temperature $kT_{\text{BB}} \sim 150$ eV.

We emphasize that this result does not indicate that there are no reflection features in the observed spectrum of Cyg X-1. As we discuss below, our ADC model with a sphere+disc geometry is able to describe the observation, and this model does include reflection. The reflection feature predicted from our model, due to reprocessing from the Comptonized continuum (which is not a pure power-law due to the contribution from the seed photons, i.e., thermal emission of the disc), differs from the feature predicted by phenomenological reflection models such as the popular *pxravl* model (Magdziarz & Zdziarski 1995), in which a pure power law is incident onto a uniform slab.

Although the residuals of our power-law fits clearly indicate the presence of an Fe K α line, the $\sim 2\%$ uncertainty in the PCA response matrix at 6 keV make a determination of the line equivalent width problematic. The division of the Cyg X-1 spectrum by a spectrum of the Crab pulsar (which is assumed to be a pure power-law) also shows that the Iron-line feature is present in our data. Due to different detector gains between the two observations, however, we cannot use the divided spectrum to estimate the equivalent width of the line. We did include a Gaussian line in most of our fits presented in Table 1. We fixed the line energy at 6.4 keV and the line-width to 100 eV [which was the typical value for the ASCA observations (Ebisawa et al. 1996)]; For all models, thawing the line-width resulted in a best-fit width of ~ 600 eV. Fitting only the line amplitude, the fits typically yielded an $EW \approx 60 \pm 35$ eV. Although undoubtedly influenced by the uncertainties in the response matrix, this EW does indicate a contribution from an intrinsic line and is probably in agreement with the results based on four days of ASCA observations presented by Ebisawa et al. (1996), who found a comparably weak Fe line with an equivalent width $EW \lesssim 30$ eV.

Thermal Comptonization is a more physical model for the observed energy spectrum of Cyg X-1. Applying the model of Titarchuk (1994) to the data, we find that a thermal Comptonization spectrum, resulting from a spherical geometry with $\tau \approx 3.6$ and $kT_c \approx 40$ keV, with an additional soft component, can give an acceptable description of the data, although the model underestimates the flux at energies $\gtrsim 150$ keV. The semi-relativistic, optically thin model (Titarchuk 1994), for either a slab geometry or a spherical geometry was unable to explain the data.

Although the traditional models can be reasonably successful in describing the observed broad band spectrum of Cyg X-1, they do not yield a physical interpretation of the emitting mechanisms responsible for the production of the

high-energy radiation. There need not be a one-to-one correspondence between a phenomenological model component and a physical interpretation. We therefore apply our self-consistent ADC models to the observed data.

3.2 Accretion Disc Corona models

For both a slab ADC model and the sphere+disc ADC model, we have computed grids of spectra using a non-linear Monte Carlo scheme based on the code of Stern et al. (1995) and modified by Dove et al. (1997a,b). The free parameters of the model are the seed optical depth τ_e , (the optical depth of the corona excluding the contribution from electron-positron pairs) and the heating rate (i.e., the compactness parameter) of the ADC. For a given compactness parameter, the temperature structure of the corona is determined by balancing Compton cooling with heating, where the heating rate is assumed to be uniformly distributed. The e^-e^+ -pair opacity is given by balancing photon-photon pair production with annihilation. Reprocessing of coronal radiation in the cold accretion disc is also treated numerically (Dove et al. 1997b)[‡]. The outer radius of the cold disc is assumed to be five times the radius of the coronal sphere ($a_r = R_d/R_c = 5$), although the results are very insensitive to the value of this ratio for $a_r \gtrsim 3$ (Dove et al. 1997b). The model spectra have been implemented into the data reduction software *XSPEC* (version 10.0) (Arnaud 1996) for use in spectral fitting. The grids of model spectra and the interpolation routines, based on Delaunay triangularization, are available upon request.

Slab-corona models do not result in good fits, as the predicted spectra are always much softer than the observed spectrum ($\chi^2_{\text{red}} \sim 80$). This result is consistent with our previous findings based on non-simultaneous data (Dove et al. 1997b). The reason that the slab ADC models always predict a spectrum softer than observed is that there is a maximum coronal temperature for a corresponding total coronal opacity. As discussed by Dove et al. (1997b), no self-consistent slab model can have *both* a high enough temperature *and* a high enough opacity to yield a Compton- y parameter large enough such that the Comptonized spectrum is as hard as that of Cyg X-1.

The sphere+disc ADC model does provide a good description of the data (cf. Table 1 and figure 6)[§]. The formal χ^2 -value of our best-fit model ($\chi^2_{\text{red}} = 1.55$) is larger than the values found for some of the phenomenological models

[‡] One improvement to the sphere+disc model, not discussed in Dove et al. (1997b), is the treatment of thermal radiation emitted by the accretion disc. Currently, the temperature of the accretion disc is assumed to be $T_{\text{BB}} \propto (R/R_c)^{-3/4}$, where R is the disc radius and R_c is the radius of the coronal sphere. The implicit flux of the disc (i.e., the radiation emitted due to viscous energy dissipation and not due to reprocessing of coronal radiation) is given by $F(R) = \sigma T^4(R)$, and the spectral shape is determined by the *local* disc temperature (a superposition of thermal Planckian distributions). Reprocessing is treated locally and is added to the intrinsic thermal flux from the disc to yield the total flux.

[§] Note that, even though the free parameters of each grid of models are the coronal seed opacity and the coronal compactness parameter, for convenience we list the corresponding *average* coronal temperature and *total* optical depth.

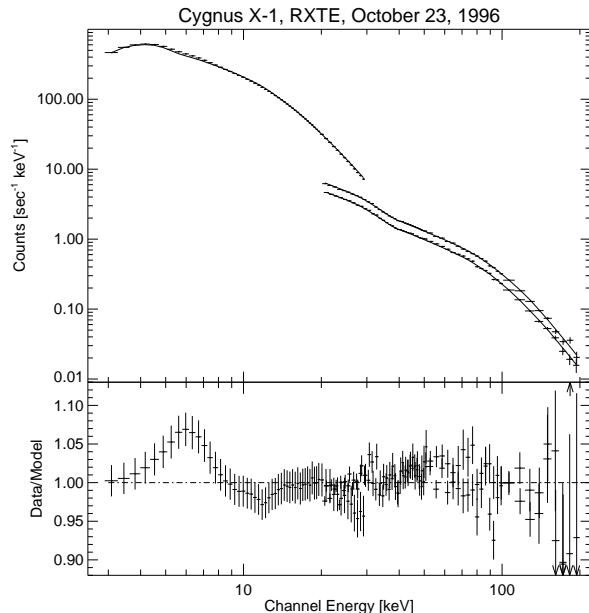


Figure 6. Top: Best-fit sphere+disc fit to the PCA and HEXTE data. Bottom: Ratio between data and model for the best-fit sphere+disc model. Deviations less than 2% are within the range of uncertainty of the PCA response matrix. Deviations in the 20 – 30 keV range are similar to those seen with best-fit models of Crab nebula observations (Jahoda, private communication).

discussed in §3.1. Considering that our model has only three parameters (seed optical depth, coronal compactness, overall normalization, plus the “hidden” parameter T_{BB} , which is fixed at 150 eV during the fitting procedure), and considering that our model is *physically self-consistent*, the level of agreement with the data is quite good. The major disagreement between the model and the data occurs in the $\approx 5 - 10$ keV range, where the residuals are as large as 7%. Below we discuss several ways in which slight modifications to our model might result in improved fits to the data.

Contrary to the results of Gierliński et al. (1997), we were able to fit the high-energy tail with a *single* Comptonizing component. This result might be due to the $\sim 15\%$ variation of the coronal temperature (due to the non-uniform radiation field and the corresponding non-uniform Compton cooling rate) in our models. We also tried sphere+disc models in which the inner temperature of the disc is 300 eV or 800 eV, the latter temperature roughly being consistent with the best-fit black-body temperature found in the previous section. However, since sphere+disc models calculate the flux emitted by the disc self-consistently, both of these models predict much more of a soft-excess than observed. This result reinforces our conclusion that the 1 keV black-body component that was added to the exponentially truncated power-law model should not be interpreted literally as disc emission.

4 DISCUSSION AND CONCLUSIONS

We have applied a variety of spectral models to an RXTE observation of Cyg X-1. We find that the observed spectrum in the 3.0–200 keV range is well described by a power-law with a photon index $\Gamma = 1.45_{-0.02}^{+0.01}$ modified by an exponential tail with an e-folding energy $E_f \approx 160$ keV, and a soft excess that was modeled as a black-body (although other broad distribution models are capable of explaining the soft-excess) having a temperature $kT_{\text{BB}} \approx 1.2$ keV. The measured value of Γ is lower than those found in previous broad-band analyses, which find a $\Gamma \sim 1.65$ (Gierliński et al. 1997; Döbereiner et al. 1994). In addition, the observed strength of the Compton reflection feature is weak, as the best-fit covering fraction, determined by fitting the data with a power-law reflection model (Magdziarz & Zdziarski 1995), is found to be ≈ 0.2 when no soft excess component is included, and is found to be $\lesssim 0.02$ when one is included. The latter value is considerably lower than the $f \approx 0.3$ found by Gierliński et al. (1997).

Two weeks prior to our observation, Cygnus X-1 transitioned from a soft (‘high’) state to a hard (‘low’) state. For a description of the properties the Cyg X-1 soft state, see Cui et al. (1997). The proximity of our observation to this transition might have influenced our results, leading to a harder spectrum and weaker reflection components than what has usually been observed from this source. However, we believe that our best-fit parameters are also due to our fitting the entire 3–200 keV spectral band, as discussed in section 3.1.

ADC models having a slab geometry are unable to explain the observed hard power-law and the small amount of reprocessing, consistent with the results of Dove et al. (1997b), Gierliński et al. (1997), and Poutanen, Krolik & Ryde (1997). In contrast, the sphere+disc ADC models provide a good explanation of the data, a result in agreement with (Gierliński et al. 1997). Furthermore these models are *physically self-consistent*. Our sphere+disc models seem to under-produce “reprocessing features,” especially the Fe line, even though reprocessing is self-consistently included within these models. For this paper, the ratio of the accretion disc radius to the coronal sphere radius, a was set to five. As shown by Dove et al. (1997b), for $a \gtrsim 5$, the geometrical covering fraction of the accretion disc, as seen from the surface of the corona, is $f_G \approx 0.30$. If these residuals, which represent less than 1% of the total flux from Cyg X-1, are due to underestimating reprocessing, several possibilities come to mind. First, our model has a sharp transition between the cold (flat) disc and the corona. It is possible that these two regions overlap to some extent, and thereby produce stronger reprocessing features. Poutanen, Krolik & Ryde (1997) suggest that these regions overlap to a large extent during the high state, which ended only two weeks prior to our observation. Another possibility is that we are observing a hot transition layer between the disc and corona. Our disc also remains flat out to its outer edge. If the disc flares, which is likely due to X-ray heating, then reprocessing features will also be enhanced. Finally, the iron abundance in the disc of Cyg X-1 could be higher than the solar value that we used in our model.

Due to the data’s broad energy range, the physical properties of the corona are well constrained. However, it is premature to claim that the sphere+disc configuration is indeed

the appropriate geometry. Other, albeit unknown, geometries in which a small fraction of coronal radiation is reprocessed by the disc, may also be able to describe the data. The spectral features due to the reprocessing of coronal radiation in the cold disc (i.e., the Fe K α fluorescence line, the Compton reflection “bump,” and the soft-excess due to thermalization of the coronal radiation) occur for energies in the $\sim 0.1 - 20$ keV range, and different geometries will predict slightly different reprocessing features. Since we had to ignore data below 3 keV, we were not able to constrain the model parameters which deal with the soft-excess due to thermal radiation emitted by the cold disc, nor can the strength or width of the iron line be directly measured (due to the uncertainty of the PCA response matrix at 5.5 keV). Therefore, more low energy data are needed to further constrain ADC models for Cyg X-1.

Additional constraints to the ADC models can come from measurements of time-lags and the temporal coherence between several energy bands from the source. These measurements can be compared with the time-lags and coherence function predicted using the physical parameters of the geometry found from spectral fitting (Vaughan & Nowak 1997; Nowak & Vaughan 1996). Only a geometry in which both the spectral and the temporal data can be explained should be considered a valid candidate for Cyg X-1. We are planning to use such an approach in a forthcoming paper.

We acknowledge the help of D. Gruber with the HEXTE data analysis, the help of K. Jahoda with the PCA response matrix, and useful discussions with I. Kreykenbohm, Ch. Reynolds, and R. Staubert. This work has been financed by NSF grants AST91-20599, AST95-29175, INT95-13899, NASA Grant NAG5-2026, NAG5-3225, NAGS-3310, DARA grant 50 OR 92054, and by a travel grant to J.W. from the DAAD.

REFERENCES

- Abramowicz, M., Chen, X., Kato, S., Lasota, J. P., & Regev, O., 1995, *ApJ*, 438, L37
- Arnaud, K. A., 1996, in *Astronomical Data Analysis Software and Systems V*, ed. J. H. Jacoby, J. Barnes, (San Francisco: Astron. Soc. Pacific) , 17
- Bałucińska-Church, M., Belloni, T., Church, M. J., & Hasinger, G., 1995, *A&A*, 302, L5
- Bałucińska, M., & Hasinger, G., 1991, *A&A*, 241, 439
- Barr, P., White, N. E., & Page, C. G., 1985, *MNRAS*, 216, 65p
- Chen, X., 1995, *MNRAS*, 275, 641
- Cui, W., Zhang, S. N., Focke, W., & Swank, J. H., 1997, *ApJ*, 484, 383
- Döbereiner, S., et al., 1994, *A&A*, 287, 105
- Done, C., Mulchaey, J. S., Mushotzky, R. F., & Arnaud, K. A., 1992, *ApJ*, 395, 275
- Dove, J. B., Wilms, J., & Begelman, M. C., 1997, *ApJ*, 487, 747
- Dove, J. B., Wilms, J., Maisack, M. G., & Begelman, M. C., 1997, *ApJ*, 487, 759
- Ebisawa, K., Ueda, Y., Inoue, H., Tanaka, Y., & White, N. E., 1996, *ApJ*, 467, 419
- Gierliński, M., Zdziarski, A. A., Done, C., Johnson, W. N., Ebisawa, K., Ueda, Y., Haardt, F., & Philips, B. F., 1997, *MNRAS*, 288, 958
- Gruber, D. E., Blanco, P. R., Heindl, W. A., Pelling, M. R., Rothschild, R. E., & Hink, P. L., 1996, *A&AS*, 120, C641
- Haardt, F., Done, C., Matt, G., & Fabian, A. C., 1993, *ApJ*, 411, L95

- Haardt, F., Maraschi, L., & Ghisellini, G., 1996, *ApJ*, 476, 670
- Hua, X.-M., & Titarchuk, L., 1995, *ApJ*, 449, 188
- Jahoda, K., et al., 1996, *BAAS*, 189, 09.06
- Magdziarz, P., & Zdziarski, A. A., 1995, *MNRAS*, 273, 837
- Narayan, R., & Yi, I., 1994, *ApJ*, 428, L13
- Nowak, M. A., & Vaughan, B. A., 1996, *MNRAS*, 280, 227
- Poutanen, J., Krolik, J. H., & Ryde, F., 1997, *MNRAS*, submitted
- Rothschild, R. E., et al., 1997, *ApJ Supp.*, in press
- Shapiro, S. L., Lightman, A. P., & Eardley, D., 1976, *ApJ*, 204, 187
- Stern, B. E., Begelman, M. C., Sikora, M., & Svensson, R., 1995, *MNRAS*, 272, 291
- Sunyaev, R. A., & Trümper, J., 1979, *Nature*, 279, 506
- Titarchuk, L., 1994, *ApJ*, 434, 570
- Vaughan, B. A., & Nowak, M. A., 1997, *ApJ*, 474, L43
- Wilms, J., Dove, J., Staubert, R., & Begelman, M. C., 1997, in *The Transparent Universe*, ed. C. Winkler, T. J.-L. Courvoisier, P. Durouchoux, (Noordwijk: ESA Publications Division) , 233
- Wu, C.-C., Eaton, J. A., Holm, A. V., Milgrom, M., & Hammer-schlag-Hensberge, G., 1982, *PASP*, 94, 149
- Zhang, W., Giles, A. B., Jahoda, K., Soong, Y., Swank, J. H., & Morgan, E. H., 1993, in *EUV, X-Ray, and Gamma-Ray Instrumentation for Astronomy IV*, ed. O. H. Siegmund, (Bellingham, WA: SPIE) , 324

Table 1. Results of spectral fitting to Cyg X-1.

Model	Γ	A_{PL}	E_{f} [keV]	kT_{BB} [keV]	A_{BB} 10^{-2}	f	kT_{C} keV	τ_{T}	A_{C}	A_{L} 10^{-3}	χ^2/dof
pl	1.70	1.78	2315/171
plexp	$1.63^{+0.01}_{-0.01}$	$1.48^{+0.03}_{-0.04}$	364^{+28}_{-25}	806/169
plexp+bb	$1.45^{+0.01}_{-0.02}$	$0.91^{+0.03}_{-0.04}$	162^{+9}_{-8}	$1.2^{+0.0}_{-0.1}$	$2.2^{+0.1}_{-0.2}$	173/167
plexp+bb+g	$1.45^{+0.02}_{-0.01}$	$0.91^{+0.04}_{-0.01}$	164^{+9}_{-8}	$1.1^{+0.1}_{-0.0}$	$2.1^{+0.2}_{-0.1}$	$3.3^{+2.5}_{-2.6}$	170/166
pextrav	$1.71^{+0.02}_{-0.02}$	$1.67^{+0.05}_{-0.06}$	924^{+400}_{-250}	$0.20^{+0.05}_{-0.05}$	752/168
pextrav+bb	$1.45^{+0.02}_{-0.01}$	$0.92^{+0.06}_{-0.05}$	164^{+10}_{-10}	$1.2^{+0.1}_{-0.1}$	$2.2^{+0.1}_{-0.2}$	$0.01^{+0.00}_{-0.01}$	173/166
pextrav+bb+g	$1.44^{+0.02}_{-0.01}$	$0.89^{+0.04}_{-0.03}$	161^{+9}_{-8}	$1.2^{+0.1}_{-0.1}$	$1.9^{+0.1}_{-0.2}$	$0.00^{+0.02}_{-0.00}$	$3.9^{+2.5}_{-2.6}$	156/165
comptt+bb	$1.1^{+0.1}_{-0.1}$	$1.4^{+0.1}_{-0.1}$...	40^{+1}_{-2}	$3.6^{+0.1}_{-0.1}$	$0.47^{+0.01}_{-0.02}$...	244/167
comptt+bb+g	$1.0^{+0.1}_{-0.1}$	$1.3^{+0.2}_{-0.1}$...	40^{+1}_{-2}	$3.6^{+0.1}_{-0.1}$	$0.47^{+0.02}_{-0.01}$	$5.9^{+2.7}_{-2.6}$	232/166
s+d	87^{+5}_{-5}	$1.6^{+0.1}_{-0.1}$	$8.07^{+0.08}_{-0.08}$...	263/169

N_{H} was fixed at $6 \times 10^{21} \text{ cm}^{-2}$. Uncertainties given are at the 90% level for one interesting parameter ($\Delta\chi^2 = 2.7$). pl: power-law with photon-index Γ and normalization A_{PL} (photon-flux at 1 keV); plexp: power-law with exponential cutoff [$A_{\text{PL}} E^{-\Gamma} \exp(-E/E_{\text{f}})$]; bb: black body with temperature kT_{BB} ; the normalization A_{BB} is defined in units of L_{39}/R_{10}^2 where L_{39} is the luminosity in units of 10^{39} erg/s and R_{10} is the distance in units of 10 kpc; pextrav: power-law with exponential cutoff reflected off cold matter (using Green's functions of Magdziarz & Zdziarski 1995), f is the ratio between the incident and the reflected flux; comptt: Comptonization spectrum after Hua & Titarchuk (1995) and Titarchuk (1994), with a coronal temperature of kT_{C} and the total optical depth τ_{T} , seed-photon temperature is 10 eV; g: Gaussian line, with energy and width fixed to 6.4 keV, 0.1 keV, respectively. A_{L} is the amplitude of the line in total number of photons/cm²/s in the line. $A_{\text{L}} = 3.3 \times 10^{-3}$ corresponds to an equivalent width of $\approx 45 \text{ eV}$. s+d: ADC model with sphere+disk geometry, total optical depth of the corona is τ_{T} , the coronal temperature is kT_{C} , the temperature profile of the cold disk is $kT_{\text{BB}}(R) = 150 (R/R_{\text{C}})^{-3/4} \text{ eV}$.